Revue RAMReS – Sciences Appliquées et de l'Ingénieur
RAMReS 2022 - *Published Online 2022* - http://publication.lecames.org/
Vol. 4(1), pp. 1-9, Online July 2022

Vol. 4
ISSN 2630-1164
June 2022

Full Length Research Paper

Energy analysis of a 30 kWe solar tower power plant for electricity production in the Sahelian zone

Kory Faye[1*], Ababacar Thiam [1, 2], Mactar Faye [1, 2]

[1]Efficiency and Energetic Systems Research Group, Alioune Diop University – Bambey, Senegal
[2]Applied Energy Laboratory, Polytechnic School, Cheikh Anta Diop University – Dakar, Senegal

Received August 2021 – Accepted January 2022

**Corresponding author. kory.faye@uadb.edu.sn*

Résumé / Abstract:
This work focuses on the energy analysis of a 30 kWe solar tower power plant for electricity production in the Sahelian zone. For this study, an indirect pressurized air volumetric solar receiver and a Capstone (C30) gas turbine are used. Thermodynamic models for each component are developed to establish the energy balance of the system and to determine its performance. A calculation code for the simulation of the solar tower power plant is developed under Matlab software by inserting all the thermodynamic models which govern the system. These calculations are made taking into account the conditions of the environment in situ, the characteristics of the solar field and the Capstone turbine. The solar field consists of 175 heliostats of 2 m^2 surface and 1.5 m height each. The results showed a solar-electrical efficiency of 25.45% for a compression ratio of 4.75 and a turbine inlet temperature (TIT) of 900 °C.

Mots clés/Keyword: Energy analysis; Solar receiver; Solar tower power plant; Capstone (C30) gas turbine.

Cite this article:
Kory Faye, Ababacar Thiam , Mactar Faye. Energy analysis of a 30 KWe solar tower power plant for electricity production in the Sahelian zone. Revue RAMReS – Sci. Appl. & de l'Ing., Vol. 4(1), pp. 1-9. ISSN 2630-1164.

1. Introduction

The electrification rate in the sub-Saharan zone is around 32% [1] on average with a strong variation from one country to another. This rate is much lower in rural areas (around 16%) where almost 70% of the population lives [1]. Moreover, most of these countries use fossil energy sources which are limited and emit greenhouse gases which are responsible for climate change [2]. Thus, with strong political support for renewable energy sources, solar energy could contribute to increase the electrification rate with off-grid or micro-grid systems [3]. It could also contribute to the reduction of fossil energy sources dependency. Solar energy can be converted into electricity via two different ways: photovoltaic (PV) technologies and concentrating solar power (CSP) technologies. Indeed, the manufacturing of photovoltaic technology is expensive and hardly exists in Africa. In addition, its electrical efficiency is still low compared to that of CSP technology [3]. Thus, the CSP technology is still considered as one of the promising ways of sustainable electricity production. The countries of the Sahel zone have a significant potential for CSP plants due to high direct normal irradiation (DNI) between 1400 and 2000 kWh/m2/year [4]

The production of electricity based on this technology is Still dominated by Dish-Stirling which have a solar-electric efficiency of 31.25% [5]. The average annual efficiency is considerably reduced by 10 to 15% due to the high maintenance costs of the Stirling engines [5]. These drawbacks limit the attractiveness of Stirling engines for the production of electricity. Thus they can be replaced by gas turbines (GT) which represent a promising technology due to their availability, reliability and low maintenance cost [6]. Moreover, they are very competitive in terms of efficiency and environmental impact. The use of gas turbines on the tower solar power plants for electricity generation has attracted much interest worldwide. They have been successfully studied and tested in some pilot projects such as Solar Two in America [7], PS10 in Spain [8] and Themis in France [9]. These plants have proven the feasibility and economic potential of this technology.

However, even of the technical feasibility of the solar tower power plant has already been demonstrated, the use of micro solar tower power plants is a new prospect for the production of electricity in rural or even remote areas. Moreover, this is the object of the project named OMSoP which was presented by Lanchi et al. [10]. In addition, this technology has been the subject of

research activities on the influence of the parameters that intervene in operation. For example, Giostri and Macchi [11] have studied the coupling of a parabolic solar concentrator with a 32.9 kWe gas turbine. An indirect cavity volumetric solar receiver was used to optimize the efficiency of conversion. The results showed solar-electric efficiencies of 26.48% and 29.11% for TIT of 900 °C and 1100 °C respectively. Giostri et al. [12] have studied a system composed of a solar tower and a micro gas turbine with power ranging between 100 and 200 kWe. A solar field of 832 m2, a compound parabolic concentrator (CPC) with an inlet diameter equal to 0.5 m and an acceptance angle of 35° inclined by 52.5° gave an optical efficiency of 77.9%. An annual solar-electrical efficiency of 16.3% is obtained for an ambient temperature of 35 °C and a DNI of 700 W/m2. Nelson et al [13] have developed and validated a quasi-stationary thermodynamic model of a 100 kWe solar tower power plant. Validation of the model at ISO conditions shows that the electrical output of the system is within 1.6% of the as-built system. The results gave an electrical efficiency of 31.5% (99.5 kWe) and a thermal efficiency of 83.2% (163.5 kWt) for a DNI of 515 W/m2. Wu et al [14] have evaluated the thermoelectric conversion performance of a solar system. The system consists of a parabolic solar collector with an alkali metal thermoelectric converter through a heat exchanger. The results showed that the efficiency could reach 20.6% for a power of 18.54 kW corresponding to an operating temperature of 1280 K. Manzoni et al [15] have developed a simulation tool for 6 kWe solar micro power plant. The simulator is used to predict the performance and ensure reliable operation of the plant when the DNI changes. The results showed a nominal peak efficiency of about 10%, which makes this solar micro power plant model attractive for the market.

Despite the few projects carried out and the studies conducted on the solar tower power plants, several operating and control challenges still exist on the various parameters involved in their operation. Moreover, to our knowledge, no realization of solar tower power plant has yet been made in the Sahelian zone where the direct normal irradiation is high and the electrification rate is still low.

This work constitutes the theoretical phase of a study for the realization of a 30 kWe solar tower power plant for electricity production in the Sahelian zone. To carry out this study, thermodynamic models for each component were developed before establishing an energy balance that will calculate the performance of the system. A calculation code is developed using Matlab software to solve all the models that govern the operation of the power plant. A parametric study is also carried out to study the effect of different key parameters on the system performance.

2. Matériels et méthodes

2.1. System layout

The system studied in this work is a 30 kWe solar tower power plant consisting of two subsystems: the solar field and the gas turbine (see Figure 1). The solar field consists of heliostats and a solar tower that carries an indirect pressurized air volumetric solar receiver (SR) at its top. The heliostats capture and concentrate the incident solar power to the receiver, which heats the working fluid (compressed air) passing through it. The gas turbine is a Capstone (C30) gas turbine single-shaft with a direct open Brayton cycle. The main change of the turbine is the replacement of the combustion chamber with the solar receiver. As a result, it consists primarily of a compressor (C), a heat exchanger (HE) and an expansion turbine (T).

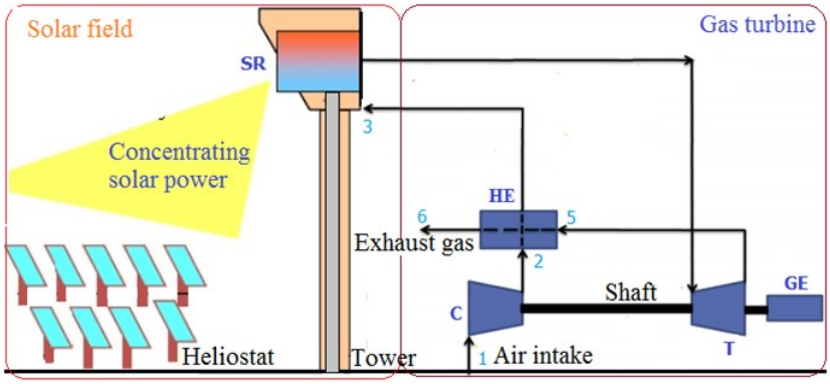

Figure 1: **Schematic diagram of the solar tower power plan**

The Brayton cycle that describes the operation of the turbine is shown in Figure 2. The ambient air is first drawn in and compressed by the compressor (1-2), then it enters in the cold side of the heat exchanger (2-3) to be preheated. After, it is heated through the solar receiver (3-4) by the concentrated solar power until the turbine inlet temperature (TIT). Then the hot gases are expanded through the turbine (4-5) to produce mechanical power on the turbine shaft which drives both the compressor and the electric generator to produce electricity. End the exhaust gases go to the hot side of the heat exchanger (5-6) to give up some of their heat to the compressed air before being sent to the outside at point 6.

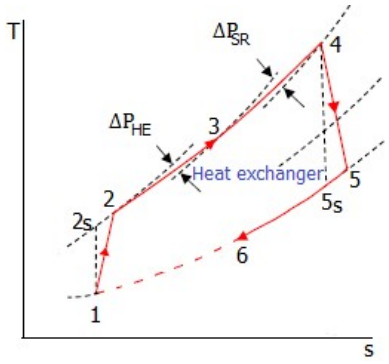

Figure 2: **Brayton cycle which describes the system**

2.2. Thermodynamic Analysis

The thermodynamic analysis of the gas turbine performance is realized by neglecting heat and pressure losses in the passages connecting the system components. The compression (1-2) and expansion (4-5) processes are assumed to be irreversible adiabatic. The thermodynamics first and second principles are used under assumed of the mass flow rate ($\dot{m}_a$) of the fluid (ambient air) is constant throughout the cycle. The ambient air is assimilated to a perfect gas with the specific heats capacities at pressure (C_p) and volume (C_v). The outlet of a component is considered as the inlet of the other component located downstream of the cycle

a Compressor

The isentropic efficiency (η_c) is a parameter that measures the degree of irreversibility of the compressor. It is defined as the ratio between the isentropic work (W_{is}) and the real work (W_r) of the compressor [16]:

$$\eta_C = \frac{W_{is}}{W_r} = \frac{h_{2is} - h_1}{h_2 - h_1} \qquad [Eq.1]$$

Compressor outlet temperature (T_2) can be calculated by the following relation:

$$T_2 = T_1\left(\frac{1}{\eta_C}(\delta_C^a - 1) + 1\right) \qquad [Eq.2]$$

Applying the first principle of thermodynamics, the real compressor work is given by:

$$W_C = \frac{C_{p1}T_1}{\eta_C}(\delta_C^a - 1) \qquad [Eq.3]$$

δ_C: Compression ratio,
C_{P1}: Specific heat capacity at a constant pressure ($JK^{-1}kg^{-1}$),
T_1: Compressor inlet temperature (K);
$a = \frac{\gamma-1}{\gamma}$.

b Heat exchanger

The heat exchanger is an essential component of the gas turbine because it allows to decrease the compression ratio while increasing the efficiency of the system [17]. In fact, it is used to preheat the compressed air by the heat of the turbine exhaust gases provided that the temperature of the compressed air (T_2) is lower than that of the exhaust gases (T_5). The heat exchanger efficiency (ε_{HE}) is defined as the ratio between the difference of temperature actually exchanged and the maximum temperature [17].

$$\varepsilon_{HE} = \frac{T_3 \quad T_2}{T_5 - T_2} \qquad [Eq.4]$$

Where T_3 is the heat exchanger outlet temperature and can be deduced by the following expression:

$$T_3 = \varepsilon_{HE}(T_5 - T_2) + T_2 \qquad [Eq.5]$$

The heat losses around the heat exchanger are neglected. Thus, the heat transfer (Q_{tr}) from the exhaust gases to the compressed air can be calculated by:

$$Q_{tr} - \dot{m}_a C_p(T_3 - T_2) \qquad [Eq.6]$$

The pressure losses on the hot side of the exchanger can be determined by the following relationship [17]:

$$\Delta P_{HE} = \frac{\rho V_e^2}{2D_h} L_{HE} f \qquad [Eq.7]$$

ρ: Density (kg/m^3).
D_h: Hydraulic diameter (m);
V_e : Flow velocity (m/s);
L_{HE} : Exchanger length (m).

The friction factor (f) can be given by this relation [6]:

$$f = (0{,}79\ln(R_e) - 1{,}64)^{-2} \qquad [Eq.8]$$

Using the definition of the hydraulic diameter, the Reynolds number can be calculated with [6]:

$$R_e = \frac{\dot{m}_c D_h (a/b)}{\mu a^2} \qquad [Eq.9]$$

a: Exchanger width (m);
b: Height of the heat exchanger channel (m);
$\dot{m}_c$: Mass flow rate of a channel (kg/s);
μ: Dynamic viscosity ($kg.m^{-1}.s^{-1}$);

c Solar receiver

The indirect pressurized air volumetric solar receiver proposed by Peter Pozivil et al [18] is chosen in this study because it meets the technical requirements imposed by the gas turbine. It can withstand temperatures up to about 1200 °C [18]. A compound parabolic concentrator (CPC) is used to minimize radiation losses and increase the concentrating solar power at the receiver inlet. The concentrated solar power is absorbed by the cavity and transmitted to the pressurized air by condition through the RPC (reticulated porous ceramic). The incident solar energy (Q_{in}) can be calculated when the total reflecting surface (S_T) of the heliostats, the optical efficiency (η_{opt}) of the solar field and the direct normal irradiance (DNI) are known.

$$Q_{in} = S_T \eta_{opt} DNI \qquad [Eq.10]$$

The solar power absorbed (Q_{ab}) is calculated by the difference between the inlet (T_3) and the outlet (T_4) temperature of the air flow.

$$Q_{ab} = \dot{m}_a C_{av}(T_4 - T_3) \quad \text{[Eq. 11]}$$

C_{av} *: Average thermal capacity at the inlet and outlet of the solar receiver* ($JK^{-1}kg^{-1}$).

Therefore, the thermal efficiency (η_{SR}) of the solar receiver can be defined as the ratio between the solar power absorbed to the solar power incident at the solar receiver.

$$\eta_{SR} = \frac{Q_{ab}}{Q_{in}} = \frac{\dot{m}_a C_{av}(T_{out} - T_{in})}{S_T \eta_{opt} DNI} \quad \text{[Eq. 12]}$$

The pressure losses (ΔP_{SR}) caused by the passage of air through the RPC is an important factor that strongly influences the performance of the system. It is calculated by the Dupuit-Forcheneimer relation through a reticulated porous material (RPC) as follows [19]:

$$\Delta P_{SR} = \left(\frac{\mu}{K} + F\rho\right) V_D L_{cav} \quad \text{[Eq. 13]}$$

K: Permeability of the porous medium (m^{-1});
F: Depuit-Forchheimer coefficient (m^2);
L_{cav}*: Cavity length (m).*

The Darcy velocity is given by the following relation:

$$V_D = \frac{\dot{m}_a}{\rho S_m} \quad \text{[Eq. 14]}$$

S_m *: Cross section of the mousse* (m^2).

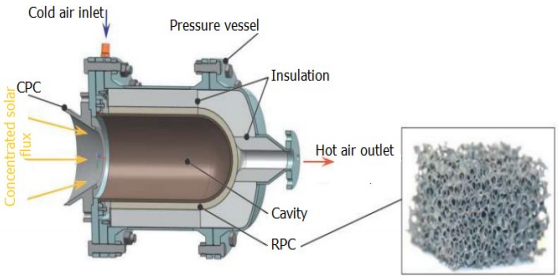

Figure 3: Section of the solar receiver cavity

d Turbine

The isentropic efficiency of the turbine (η_T) is defined as the ratio between the real work (W_r) and the isentropic work (W_{is}). It is calculated by the following relation.

$$\eta_T = \frac{W_r}{W_{is}} = \frac{h_5 - h_4}{h_{5s} - h_4} \quad \text{[Eq. 15]}$$

The turbine outlet temperature (T_5) can be determined by the following relationship:

$$T_5 = T_4(\eta_T(\delta_C^{-a} - 1) + 1) \quad \text{[Eq. 16]}$$

The turbine mass work (W_T) is given by the following relation:

$$W_T = C_{p2}\eta_T T_4(\delta_C^{-a} - 1) \quad \text{[Eq. 17]}$$

C_{p2}*: Specific heat capacity of the gas* ($JK^{-1}kg^{-1}$).

e Energy balance

The energy balance determines the performances of the turbine. Thus, the thermal efficiency (η_{Th}) is defined as the ratio between the net work (W_{net}) and the thermal power (Q_{th}) of the system, that is to say:

$$\eta_{Th} = \frac{W_{net}}{Q_{th}} \quad \text{[Eq. 18]}$$

Or the net work is the difference between the work produced by the turbine (W_T) and the work used by the compressor (W_C).

$$W_{net} = W_T - W_C \quad \text{[Eq. 19]}$$

The electrical work of the turbine (W_{el}) is the product of the net work and the electrical efficiency of the generator (η_g).

$$W_{el} = (W_T - W_C)\eta_g \quad \text{[Eq. 20]}$$

Then the solar-electrical efficiency (η_{sol-el}) defined as the ratio between the electrical work and the solar power absorbed by the receiver can be determined by:

$$\eta_{sol-el} = \frac{W_{el}}{Q_{ab}} \quad \text{[Eq. 21]}$$

2.3. Operating parameters

The performance calculation of the solar power plant requires the definition of the ambient conditions of the in situ zone. The atmospheric temperature and pressure are assumed to be equal to 25 °C and 101325 Pa respectively. The relative humidity of the air is equal to 60% for gas turbines. The operating parameters of the Capstone turbine (C30) represent its characteristics (see Table 1) [20]. They are used to determine the system performances.

Table 1: Capstone turbine (C30) characteristics

Parameters	Values	Units
Nominal power	30	[kWe]
Net power output	28(±2)	[kWe]
Electrical efficiency	0.26(±2)	[-]
Turbine inlet temperature	1173	[K]
Exhaust mass flow	0.31	[kg/s]
Rotation speed	96,000	[rpm]
Pressure ratio	3.45	[-]
Exhaust gas temperature	548	[K]
Compressor isentropic efficiency	0.78	[-]
Turbine isentropic efficiency	0.80	[-]
Heat exchanger efficiency	0.877	[-]

The solar field sizing results for the 30 kWe solar tower power plant found in our previous studies are used in this work. The optical efficiency of the field was 76.4% for a reference DNI of 600 kW/m^2. The total reflective area of the heliostats is 350 m^2. The solar field is composed of 175 heliostats. Each heliostat has a reflective surface of 2 m^2 and a height of 1.5 m. The characteristics of the different subsystems of the solar field are represented in this table.

Table 2: Characteristics of the solar field subsystems

Parameters	Values	Units
Héliostat		
Total reflective area	350	[m^2]
Heliostat number	175	[-]
Reflective surface per heliostat	2	[m^2]
Heliostat height	1.5	[m]
Solar Receiver		
CPC inlet aperture diameter	0.7	[m]
Cavity inner diameter	0.25	[m]
Cavity diameter	0.5	[m]
Cavity length	0.5	[m]

A simulation code is performed by inserting all the thermodynamic models that govern the system operation into a Matlab software. The simplified flowchart of the system performance calculation model is shown in Figure 4. Firstly, the model calculates the compressor work (W_C) and the compressor outlet temperature (T_2). Then, the exchanger outlet temperature (T_3), the heat exchanged (Q_{tr}), and the pressure losses (ΔP_{HE}) of the heat exchanger are evaluated. After that, the incident solar power (Q_{in}), the absorbed solar power (Q_{ab}) and the pressure losses (ΔP_{SR}) in the solar receiver are determined before calculating the turbine work (W_T) and the turbine outlet temperature (T_5). Finally, the thermal and electrical efficiencies of the system are obtained. These calculations are realized taking into account the ambient conditions, the solar field data and the characteristics of the Capstone turbine (C30).

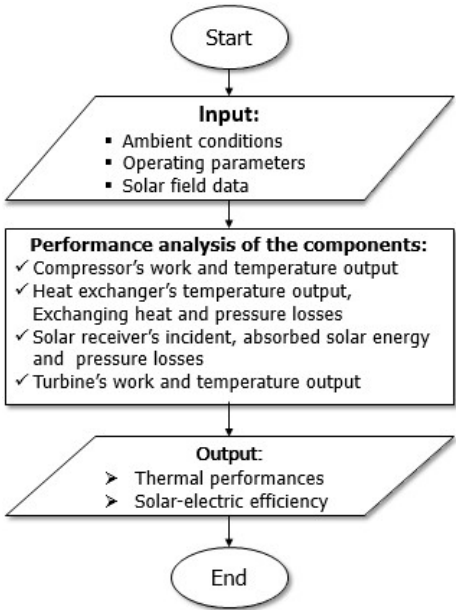

Figure 4: **Simplified flowchart of performance calculations**

3. Results and discussions

3.1. DNI in Senegal

Figure 5 shows the direct normal irradiation (DNI) measured for some months of the year in Senegal. A reference DNI of 600 W/m² on march 21, was used for the solar field sizing and allowed to obtain an operating range of about 6 hours. These DNI data show the intermittent of the solar source, which has a strong influence on the performance of the solar tower power plant.

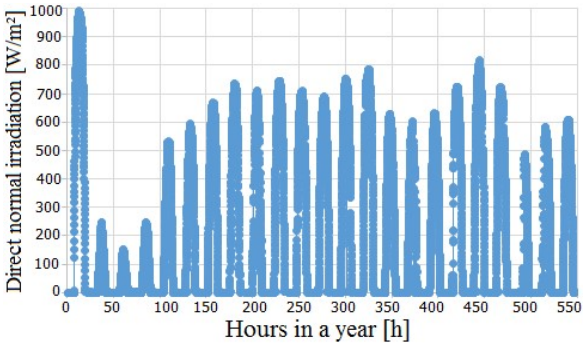

Figure 5 : **Direct normal irradiation in Senegal**

3.2. Performances of the components

In this section, the performance results of the system components are presented. Figure 6 shows the variation of the compressor outlet temperature (T_2) as a function of the compressor ratio (δ_C) for different ambient temperatures (T_1). The minimum ambient temperature (T_1) is taken at 25 °C and the maximum at 45 °C. As shown in this figure, the compressor outlet temperature increases with the compression ratio and the ambient temperature. Figure 7 shows the turbine outlet temperature (T_5) as a function of the compressor ratio for different turbine inlet temperatures (TIT=T_4). The minimum and maximum TIT are 800 °C and 950 °C respectively. It can be seen that, the turbine outlet temperature (T_5) decreases with increasing the compressor ratio but increases with turbine inlet temperature. Indeed, the compressor ratio is inversely proportional to the expansion ratio (δ_T), which leads to a decrease of the temperature T_5

The pressure losses (ΔP_{HE}) as a function of the mass flow rate ($\dot{m}_a$) of the pressurized air for different lengths of the heat exchanger are shown in figure 8. It can be seen that the pressure losses increase with the mass flow rate and the heat exchanger length. This is due to the increase in air velocity and the different friction it experiences on the walls of the exchanger. Considering the operating mass flow rate of the turbine which is 0.3 kg/s, the pressure losses in the heat exchanger are 8,334 mPa at 25 cm length.

The pressure losses (ΔP_{HE}) as a function of the mass flow rate ($\dot{m}_a$) of the pressurized air for different lengths of the heat exchanger are shown in figure 8. It can be seen that the pressure losses increase with the mass flow rate and the heat exchanger length. This is due to the increase in air velocity and the different friction it experiences on the walls of the exchanger. Considering the operating mass flow rate of the turbine which is 0.3 kg/s, the pressure losses in the heat exchanger are 8,334 mPa at 25 cm length.

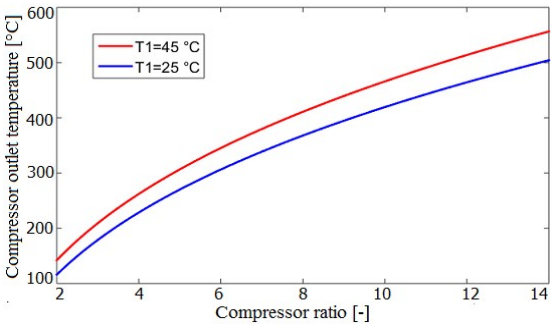

Figure 6 : Compressor outlet temperature via compressor ratio for different T_1

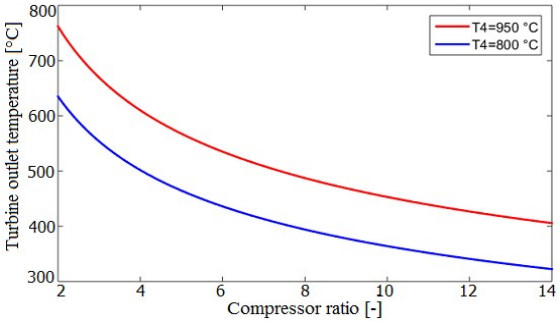

Figure 7 : Tutbine outlet temperature via compressor ratio for different TIT

These results are obtained by neglecting the thermal resistance of the plates that constitute the exchanger. Figure 9 shows the pressure losses (ΔP_{SR}) across the RPC of the solar receiver as a function of the air mass flow rate for different diameters of the cross-section (Ds) of the RPC mousse. As shown in this figure, the pressure losses increase with increasing mass flow rate and decreasing mousse cross-sectional diameter. The pressure loss is 163.2 mPa for a mass flow rate of 0.3 kg/s and a cross-sectional diameter of 75 mm. This value corresponds to a static pressure loss of 3.38%, which is still relatively low compared to combustion turbines whose static losses can reach 8%.

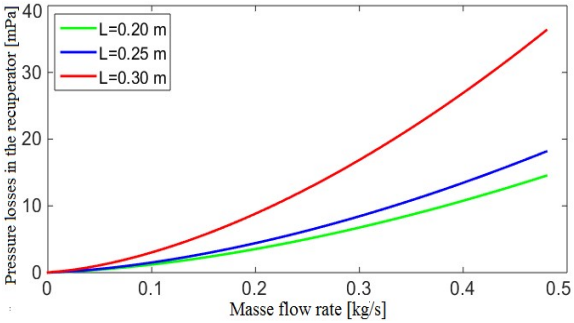

Figure 8 : Pressure losses via mass flow for different exchanger lengths

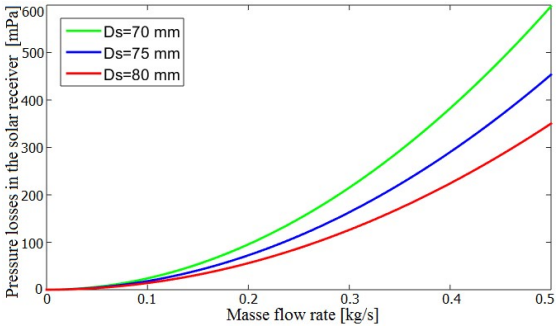

Figure 9 : Pressure losses via mass flow rate for different diameters of the RPC section

3.3. Performances of the system

Figure 10 shows the net thermal efficiency ($\eta_{net,th}$) as a function of the specific work (W_{sp}) of the turbine for different TIT. The minimum TIT is set at 800 °C while the maximum is at 950 °C. The net thermal efficiency increases with the specific work until the optimum value where it starts to decrease. On the other hand, the increase of the turbine inlet temperature leads to both the increase of the efficiency and the corresponding optimal specific work. Therefore, for a TIT of 900 °C, the optimal value of the efficiency is equal to 35.89% for a specific work of 247.6 kJ/kg.

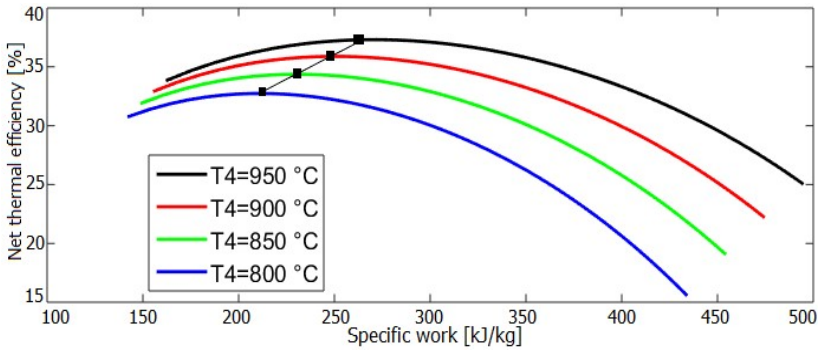

Figure 10: **Net thermal efficiency via specific work for different TIT**

The thermal efficiency (η_{Th}) of the turbine as a function of the compressor ratio for different TIT is shown in Figure 11. The thermal efficiency increases up to a threshold value of the compressor ratio where it starts to decrease. Furthermore, this efficiency is higher when the TIT is increased. However, increasing the turbine inlet temperature can also increase the optimum compressor ratio, which can cause the turbine to burn out. Thus, a thermal efficiency of 38.3% is obtained for a compressor ratio of 3.56 and a TIT of 900 °C.

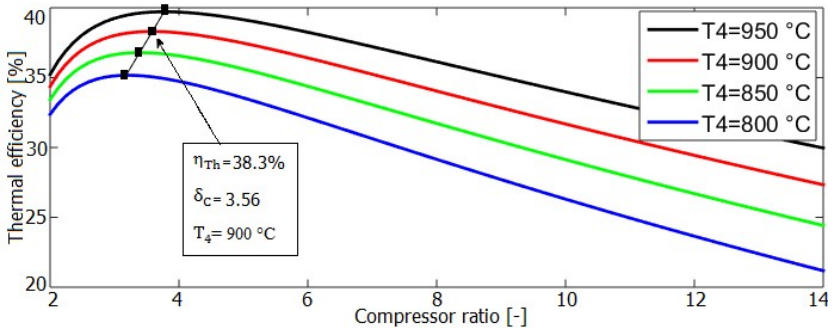

Figure 11: **Thermal efficiency via compressor ratio for different TIT**

In addition, the increase in turbine inlet temperature (TIT) causes some changes in the expansion valve and heat exchanger, which must confront with different operating temperatures than under conventional conditions. As shown in Figure 12, the temperature (TIT) is proportional to the thermal efficiency of the turbine. Therefore, it is important to control the turbine inlet temperature because excessive increases can lead to destructive thermal stresses in the turbine materials.

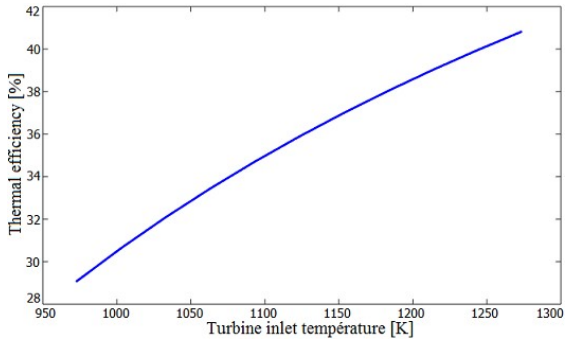

Figure 12: **Thermal efficiency via turbine inlet temperature**

The influences of turbine inlet temperature (TIT) and compressor ratio on solar-electrical efficiency are evaluated and represented in Figure 13. The trend is similar to that found for the thermal efficiency as the solar-electric efficiency increases with the compressor ratio until an optimum value is reached where it starts to decrease. It can also be seen that the increasing of the TIT leads to both the increase in the optimum efficiency and the corresponding compressor ratio. As can be seen in this figure, an optimum solar-electric efficiency of 25.45% is obtained for a compressor ratio of 4.76 and a TIT of 900 °C. This result is close to the reality, i.e. the electrical efficiency of the Capstone (C30) turbine which is equal to 26% for a compressor ratio of 3.4 and a TIT of 900 °C. Table 3 shows also a comparison between the results of this study and those found in Giostri et Macchi [11].

Table 3: Comparison between the simulation results and the results of Giostri et Macchi [11

Parameters	P_e	TIT	δ_C	η_{sol-el}
Present study	30 kW	900 °C	4.74	25.45%
Giostri et Macchi [11]	32.9 kW	900 °C	3.3	26.48%

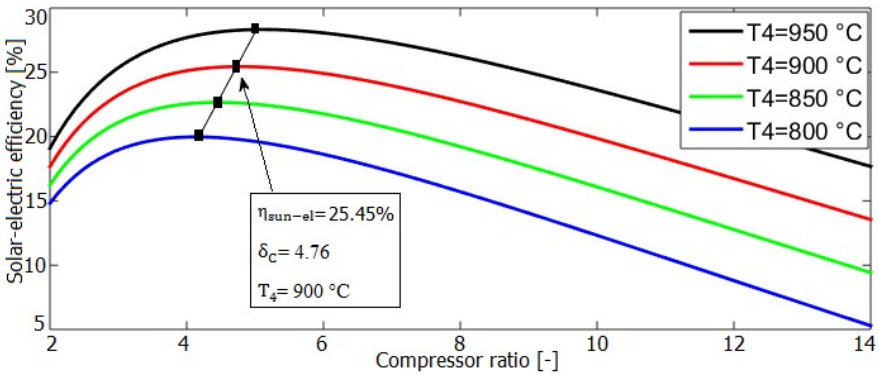

Figure 13: **Solar-electrical efficiency via compressor ratio for different TIT**

Figure 14 determines the distribution of input (or output) temperatures for each component of the system. The turbine inlet temperature (i.e. the receiver outlet temperature, T_4) represents the operating

temperature of the turbine. The turbine outlet temperature (T_5) is higher than the compressor outlet temperature (T_2), which is why the heat exchanger plays an important role. Apart from the temperature T_4, the temperature T_5 is higher followed by the heat exchanger outlet temperature (T_3). Moreover, we can see that the temperature (T_2) is higher than that of the gases released into the atmosphere (T_6). T_1 is the ambient temperature, i.e. the compressor inlet temperature.

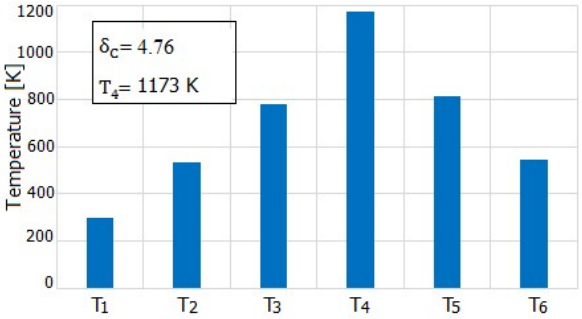

Figure 14: **Temperatures of system components**

Table 4 summarizes the different simulation results of the solar power plant operation. These results are obtained taking into account the ambient conditions (T_1= 25 °C, P_1=1.01325 atm), the solar field data and the characteristics of the Capstone turbine (C30).

Table 4: Simulation results of the solar tower power plant

Parameters	Values	Units
Work to drive the compressor	235.72	[kJ/kg]
Compressor outlet temperature	533.7	[K]
Recuperator pressure losses	8.334	[mPa]
Available solar energy	160.44	[kW/m²]
Receiver impinging power	128.35	[kW/m²]
Recuperator outlet temperature	778.4	[K]
Receiver pressure losses	163.2	[mPa]
Receiver outlet temperature	1173	[K]
Turbine work	-382.05	[kJ/kg]
Turbine outlet temperature	814.9	[K]
Turbine specific work	247.6	[kJ/kg]
Exhaust gas temperature	548	[K]
Net work	146.33	[kJ/kg]
Net electrical work	131.69	[kJ/kg]
Thermal efficiency	38.3	[-]
Compression ratio	4.76	[-]
Solar-electrical efficiency	25.45	[-]

4. Conclusion

In this study, we performed an energy analysis of a 30 kWe solar tower power plant for electricity production in the Sahelian zone. An indirect pressurized air volumetric receiver and a Capstone (C30) turbine were chosen because of their performance and the availability of their design characteristics. Thermodynamic models for each component were developed to establish an energy balance that will calculate the performance of the system. The simulation results showed a solar-electrical efficiency of 25.45% for a compressor ratio of 4.76 and a TIT of 900 °C. However, due to the solar source intermittent (see Figure 5), it will be difficult to ensure stable power production from stand-alone solar power plants. But this problem can be overcome by hybridizing these plants with other energy sources. It is also noted that the temperature of the gases released into the atmosphere (548 K) is still high, the cogeneration will allow to obtain heat for further use. All these show that solar power plants are promising technologies for decentralized electricity production.

Acknowledgements

We thank all the members of the organizing committee of the 2nd West African Renewable Energy Conference (CAO-ER2020) for giving us the opportunity to participate in this conference and to be among the winners

REFERENCES

[1] I. Onyeji, M. Bazilian, P. Nussbaumer, Contextualizing electricity access in sub-Saharan Africa, Energy for Sustainable Development, Vol. 16, pp. 520–527, 2012.

[2] Daabo et al. Development of three dimensional optimization of a small-scale radial turbine for solar powered Brayton cycle application, Applied Thermal Engineering, Vol. 16, pp. 718–733, 2017.

[3] K. E. N'Tsoukpoe, K. Y. Azoumah, E. Ramde and al. Integrated design and construction of a micro-central tower power plant, Energy for Sustainable Development, Vol.31, pp.1-13, 2016.

[4] A. Thiam, C. Mbow, M. Faye, P. Stouffs and D. Azilinon, Assessment of hybrid concentrated solar power-biomass plant generation potential in Sahel: case study of Senegal, Natural Resources, Vol. 8, pp. 531-547, 2017.

[5] Mohamed Abbas et al. Dish Stirling Technology: A 100 MW solar power plant using hydrogen for Algeria, International Journal of Hydrogen Energy, Vol. 36, pp. 4305-4314, 2011.

[6] Roux et al. The efficiency of an open-cavity tubular solar receiver for a small-scale solar thermal Brayton cycle, Energy Conversion and Management Vol. 84, pp. 457-470, 2014.

[7] James E. Pacheco et al., Final Test and Evaluation Results from the Solar Two Project, Solar Thermal Technology, Sandia National Laboratories, 2002

[8] M. A. Mustafa, S. Abdelhady, A. A. Elweteedy, Analytical Study of an Innovated Solar Power Tower (PS10) in Aswan, International Journal of Energy Engineering, Vol. 2(6), pp. 273-278, 2012

[9] B. Bonduelle, B. Rivoire and A. Ferriere, La centrale expérimentale THEMIS : Bilan et Perspectives, Revue de Phys. Appl., 1989.

[10] Lanchi et al. Investigation into the coupling of micro gas turbine with CSP-technology: OMSoP Project, Energy Procedia, Vol. 69, pp. 1317-1326, 2015.

[11] Giostri and Macchi. An advanced solution to boost sun-to-electricity efficiency of parabolic dish, Solar Energy, Vol. 139, pp. 337-354, 2016.

[12] Giostri et al. Small scale solar tower coupled with micro gas turbine, Renewable Energy, Vol. 147, pp. 570-583, 2020.

[13] Nelson et al. Thermodynamic modeling of solarized micro turbine for combined heat and power applications, Applied Energy, Vol. 212, pp. 592-606, 2018.

[14] Shuang-Ying Wu, Lan Xiao, Yiding Cao and You-Rong Li, A parabolic dish/AMTEC solar thermal power system and its performance evaluation, Applied Energy, Vol. 87, pp. 452–462, 2010.

[15] Stefano Mazzoni, Giovanni Cerri and Leila Chennaoui, A simulation tool for concentrated solar power based on micro gas turbine engines, Energy Conversion and Management, Vol. 174, pp. 844–854, 2018.
[16] A. Javanshir, Nenad Sarunac and Zahra Razzaghpanah, Thermodynamic analysis of simple and regenerative Brayton cycles for the concentrated solar power applications, Energy conversion and management, Vol. 163, pp.428-443, 2018.
[17] Maghsoudi et al. Comparative study and multi-objective optimization of plate-fin recuperator applied in 200 kW micro turbines based on non-dominated sorting and normalization method considering recuperator effectiveness, exergy efficiency and total cost, International Journal of Thermal Sciences, Vol. 124, pp.50-67, 2018.
[18] Peter Pozivil, Simon Ackermann and Aldo Steinfeld, Numerical Heat Transfer Analysis of a 50 kWth Pressurized-Air Solar Receiver, Journal of Solar Energy Engineering, Vol. 137, 2015.
[19] Petrasch et al. Tomography based determination of permeability, Dupuit–Forchheimer coefficient, and interfacial heat transfer coefficient in reticulate porous ceramics, International Journal of Heat and Fluid Flow, Vol. 29, pp. 315-326, 2008.
[20] C30 Micro Turbine Natural Gas, Available from www.capstoneturbine.com,